RAD Conference Proceedings, vol. 7, pp. 79-85, 2023
ISSN 2466-4626 (online) | DOI: 10.21175/RadProc.2023.15
www.rad-proceedings.org

THREE-DIMENSIONAL COMPUTATIONAL FLUID DYNAMICS INVESTIGATION OF THE DISPERSION OF RADIOACTIVE CLOUD

Giuseppe Giannattasio[1*], Alessio Castorrini[2], Antonio D'Angola[1] , Michele Ferrarini[3], Francesco Bonforte[1,3]

[1]Università degli Studi della Basilicata, Potenza, Italy
[2]Sapienza Università di Roma, Rome, Italy
[3]Fondazione CNAO, Pavia, Italy

Abstract. *The evaluation of spatial distributions of plume dispersion into the atmosphere is an important task for estimating the release of radioactive gas. The Gaussian Plume Model represents the most adopted implementation for submersion dose evaluations from an emission stack. The radioactive cloud dispersion is obtained by calculating the Briggs' coefficients that varies with the meteorological conditions, mainly the wind speed and the atmosphere stability. The ideal scenarios for these models are installations located far away from urban areas, such as nuclear power or big industrial plants. On the other hand, healthcare facilities, such as nuclear medicine, radiotherapy suites or hadrontherapy accelerators, are usually situated in populated areas and in close vicinity to other buildings. For this reason, the hypotheses of the GPM cannot be applied without corrections, since the pollutant transport is affected by several phenomena (buoyancy, downwash) due to the buildings. CFD model can provide a reliable estimate of the pollutant distribution that take into account all these effects. In this work, comparisons between Gaussian plume and fluid dynamic models are performed in order to make comparison at short and long distances. Fluid dynamic results have been obtained by solving the steady-state Reynolds Averaged Navier-Stokes equations using the k-ω turbulence closure model, which has been modified to account for atmospheric stability, thermal stratification, and ground roughness effects. The Monin-Obukhov Similarity Theory is employed to define consistent inflow conditions to simulate different levels of atmospheric stability. Numerical results have been obtained by considering different stability atmospheric conditions and comparisons and differences between models are presented and discussed. Once a reliable distribution of the radioactive pollutant is known, several dosimetric approaches can be adopted in order to evaluate the doses received by population (e.g. Monte Carlo evaluation of the submersion dose, multiplication of the concentration by the screening factors).*

Keywords: *Computational Fluid Dynamics, Radioactive clouds, Atmospheric Boundary Layer, Atmospheric Stability, Monin Obukhov Similarity Theory, Turbulence, Gaussian Plume Model.*

1. INTRODUCTION

The study of the transport of gaseous pollutants into the atmosphere in the proximity of urban areas is becoming particularly important in the light of the environmental impact assessment requirements imposed by current legislation on prevention and safety for the population. The health implications are then obviously related to the type of pollutants, usually source of chemical risk but also of ionizing radiation produced by radioactive substances, for example as a consequence of the operating cycles of the particle acceleration machinery provided by centers of Nuclear Medicine and therapy centers for oncological treatments, usually situated in the proximity of urban agglomerations. To address the analysis of such environmental diffusion scenarios both in open and urban areas, simplified model, as the Gaussian Plume Model (GPM), can be used or, alternatively, numerical simulations of more accurate fluid dynamic model can be carried out. As an example, it is possible to use accurate computational fluid dynamics (CFD) techniques by using complex and time consuming grid generation. GPM can result effective in some particular cases and at long distance from the source emission. In contrast, CFD simulations can be particularly indicated in presence of buildings and obstacles. Moreover, in the CFD methodology, the effect of turbulence, which is related to different atmospheric conditions, can be accurately described by recurring to different dispersion models. Typically, in the framework of CFD model, a good approximation is provided by Navier-Stokes equations averaged by Reynolds (RANS), in which proper boundary conditions take into account different windy regimes and characteristics of the territory (valley or plain) [1]. CFD approaches it might be suitable in particular for urban areas in which results obtained by simplified models could be affected by unacceptable approximations due to the presence of the surrounding buildings, since they always significantly modify the distribution curves of the effluent concentrations obtained in the open and unhindered fields [2]. Within the RANS framework, the effect of different atmospheric conditions and turbulent phenomena can be described by recurring to different theoretical approaches such as the k-ε and k-ω models, in which k is the turbulent kinetic energy, ε the turbulent kinetic energy dissipation and ω the

* E-mail of the corresponding author – giuseppe.giannattasio@unibas.it

dissipation rate. In the present paper, transport phenomena of gaseous pollutants have been investigated by using a CFD model in turbulent regime in order to consider different stability atmospheric conditions. Numerical results have been obtained by considering different turbulent theoretical approaches. Comparisons and differences between GPM and CFD models are presented and discussed. The effectiveness of the Shear Stress Transport (SST) variant of the *k-ω* model will be highlighted as the appropriate approach to investigate scenario changing with atmospheric conditions.

2. GAUSSIAN PLUME EQUATION

The standard Gaussian Plume equation used in the theory of Pasquill [3] for evaluating the concentration $C(x,y,z,t)$ of a gas or an air pollutant emitted continuously from a source is given by the following equations [3-6]

$$C = \frac{Qe^{-\frac{y^2}{2\sigma_y^2}}}{2\pi U\sigma_y\sigma_z}\left[e^{-\frac{(z-H_s)^2}{2\sigma_z^2}} + e^{-\frac{(z+H_s)^2}{2\sigma_z^2}}\right] \quad (1)$$

where H_s, Q, U, σ_z, σ_y are the effective source height, the continuous source emission rate of the pollutant, the mean transport wind speed in the direction of the *x* axis and the diffusion parameters in the corresponding directions, respectively. Equation (1) can be obtained as the analytical solution of a simplified diffusion equation under the assumption of Gaussian distributions of the pollutant in the direction normal to the drift of the plume. Different models [4, 6] can be adopted for the dispersion diffusion parameters, both in open fields or including the effect of buildings [4]. Briggs expressions are widely adopted and are expressed as a function of the distance by the source *x* by the following expressions [6]

$$\sigma_y = ax(1+cx)^{0.5} \qquad \sigma_z = ax(1+cx)^d \quad (2)$$

where *a*, *c* and *d* are coefficients which depend on the surroundings and the stability class of the atmosphere [6]. GPMs prove to be effective at long distance from the source but could be affected by unacceptable errors at lower distance. For this reason, in the present paper a deeper investigation has been carried out by using CFD approach, as described in the following sections. A comparison between Pasquill and CFD results are reported in the following sections.

3. COMPUTATIONAL FLUID DYNAMICS MODEL OF CLOUD DISPERSION

3.1. RANS and turbulence models

The CFD model is based on the solution of the pressure-based (incompressible) Reynolds-Averaged Navier-Stokes equations. The effects of the vertical temperature profile and non-uniform temperature distribution are accounted for using the Boussinesq approximation, which states that density variations have a non-negligible effect in the momentum equations only in relation to the buoyancy force. This approach allows for the retention of the incompressible model and simplifies the energy equation to a temperature transport equation.

Two-equation eddy-viscosity models based on turbulent kinetic energy, *k*, are typically selected for turbulence closure in Atmospheric Boundary Layer (ABL) RANS simulations. According to works as [7] and [8], *k-ε* and *k-ω* models, integrated with an appropriate selection of boundary condition modelling for inflow and terrain, can accurately describe the ABL in a RANS simulation.

Among others, the Shear Stress Transport (SST) variant of the *k-ω* closure equations [9] has been selected for this study. This model provides a reasonable choice as it has historically shown good accuracy in resolving near flow fields, important for resolving smaller scale flow features close to the chimney walls, while retaining the ability of the *k-ε* model to solve the far-field ABL profile [10]. The model also accounts for the buoyancy effect due to thermal gradients through a source term included in the *k* equation (e.g. see [11]).

3.2. Atmospheric Boundary Layer Stability: the Monin-Obukhov Similarity Theory

As previously mentioned, accurate resolution of the ABL in a RANS simulation requires the imposition of appropriate and consistent boundary conditions for velocity, turbulence, and temperature. The Monin-Obukhov Similarity Theory (MOST) [12] is commonly used to account for different stability conditions in the atmospheric surface layer. According to MOST, it is possible to derive the following vertical profiles to be applied as boundary conditions for the Reynolds averaged velocity *u(z)*, temperature *T(z)*, and for the turbulent kinetic energy *k(z)* and dissipation rate *ε(z)*:

$$u(z) = \frac{u_*}{\kappa}\left[\ln\left(\frac{z}{z_0}\right) - \psi_m\left(\frac{z}{L}\right)\right] \quad (3)$$

$$T(z) = T(z_0) + \frac{T}{\kappa}\left[\ln\left(\frac{z}{z_0}\right) - \psi_t\left(\frac{z}{L}\right)\right] \quad (4)$$

$$k(z) = \frac{u_*^2}{\sqrt{C_\mu}}\psi_k\left(\frac{z}{L}\right) \quad (5)$$

$$\varepsilon(z) = \frac{u_*^3}{\kappa z}\psi_\varepsilon\left(\frac{z}{L}\right) \quad (6)$$

being $\psi_k = \sqrt{\psi_\varepsilon/\psi_m}$ and where z_0 is the roughness parameter, u_* is the friction velocity, κ is the Von Karman constant and the functions ψ are the stability-related functions defined according to MOST [13] as follows:

$$\psi_m\left(\frac{z}{L}\right) = \psi_t\left(\frac{z}{L}\right) = -5\left(\frac{z}{L}\right) \quad (7)$$

$$\psi_m\left(\frac{z}{L}\right)=\psi_t\left(\frac{z}{L}\right)=0 \quad (8)$$

$$\psi_m\left(\frac{z}{L}\right)=2\ln\left[\frac{1+\rho(z)}{2}\right]+\ln\left[\frac{1+\rho^2(z)}{2}\right] - 2\arctan[\rho(z)]+\frac{\pi}{2} \quad (9)$$

$$\psi_t\left(\frac{z}{L}\right)=2\ln\left[\frac{1+\rho^2(z)}{2}\right] \quad (10)$$

$$\rho\left(\frac{z}{L}\right)=\left(1-16\frac{z}{L}\right)^{1/4} \quad (11)$$

(7)-slightly stable, (8)-neutral, (9, 10)-slightly unstable

The functions ψ are based on the Monin-Obukhov length L, a parameter that characterizes the stability state of the surface layer. In particular, when $L<0$, the surface layer is statically unstable, dominated by buoyant processes; when $L>0$, it is statically stable and finally under neutral conditions, $L\to\infty$. The correlation between the value of z_0, L and the Pasquill stability classes can be found in [14].

3.3. Geometry, numerical implementation and model setting

The domain under investigation is represented by a 3D rectangular prism with L_x=1.5 km, L_y=1 km and L_z=1 km, being x the wind direction. In the domain, a chimney of cylindrical shape (height H= 102.2 m and radius R=1 m) has been included at (x=0.5 km, y=0.5 km, z=0).

An unstructured hybrid mesh with local refinement regions has been generated to solve the plume transport region and the flow field close to the ground and the chimney. In particular, a horizontal volume has been introduced for a more accurate calculation sensitivity. The volume, indicated as Body of Influence (BOI), is represented in Fig. 1 and has a cylindrical shape. The radius of BOI r=100 m and its z coordinate has been selected in order to follow accurately the contaminant transport phenomena starting from the values given by the Pasquill theory. Its resolution has been selected on the basis of numerical convergence of the flow concentrations with a 2 m minimum element size. The model has been implemented in the framework of Ansys Academic Research CFD 2023 R1 with boundary conditions given in Table 1.

Table 1. Boundary conditions of the domain

Face	Type
Inlet_chimney	*velocity_inlet*
Inlet_wind	*velocity_inlet*
Outlet_wind	*outflow*
Outlet_sides	*symmetry*
Farfield_upper	*velocity_inlet*
Bottom surface	*wall*

Preliminary numerical simulations have been carried out in order to verify the numerical model. In particular, the simulation of the wind field for different stability classes has been performed with both k-ε and k-ω SST models in the absence of a chimney, and comparing the results with the vertical profiles computed and reported in [10]. In this test, both models maintain the horizontal homogeneity of the velocity field, recording negligible differences with the reference data in [10] and demonstrating their capability to solve the ABL profile consistently with the MOST based inflow conditions. However, when the chimney structure is added to the domain, the k-ε based setup resulted in much higher values of turbulent viscosity, making the solution significantly dependent on the maximum turbulent viscosity ratio threshold, which is a limiter required for numerical stability. This parameter sets the limiting maximum allowable value during simulations of the ratio of turbulent to laminar viscosity, by default set at 10^5 [15]. As an example, Figure 2 reports results obtained for Argon concentration distribution for stability class D at x = 200 m as a function of z. The k-ω SST setup did not show significant dependency on the turbulent viscosity ratio threshold, which has been properly modified in the range 10^4-10^6, making k-ω SST model the most appropriate approach for this study.

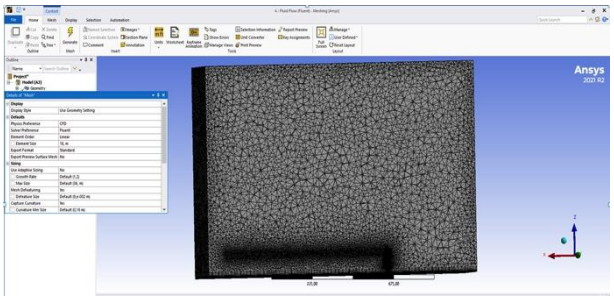

Figure 1. BOI's model (meshing).

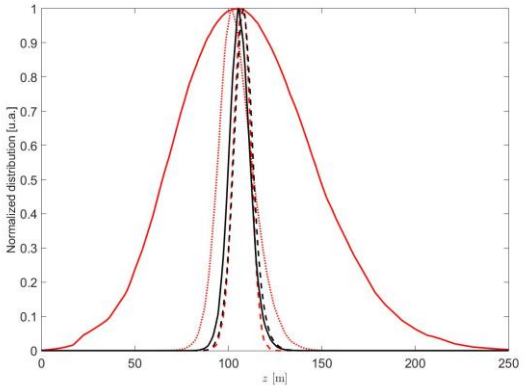

Figure 2. Argon concentration distribution for stability class D at x = 200 m. Turbulence parameter: for the k-ε model: 10^6 full red line, 10^5 dotted red line, 10^4 dashed red line. For the k-ω model: 10^5 full black line, 10^6 dashed black line.

4. NUMERICAL RESULTS

Numerical results have been obtained by considering different stability atmospheric conditions. Comparisons between the Gaussian Plume Model and CFD turbulent model are presented and discussed. The box is filled with air and an air/Argon mixture (5% in mass of contaminant Argon) has been inserted by the chimney in the domain with a velocity inlet of 5 m/s. In order to simulate different stability classes, wind velocity, wind frictional velocity and temperature length scale given in Table 2 have been considered. These last two parameters of wind and temperature are required by the CFD-simulation to set the MOST profiles. They were derived, for each stability class, from experimental data [10]. Numerical concentrations of Argon have been gathered on four planes orthogonal to wind direction (x) and placed at downstream distance d = 25 m, 50 m, 100 m and 200 m from the chimney position, as shown in Figure 3.

Table 2. Stability classes, wind velocities [m/s] and Temperature length scale [K]

Stability Class	Wind velocity	Wind frictional velocity	Temperature length scale [K]
C (slightly unstable)	7.55	0.42	303.6
D (neutral)	4.29	0.22	294.2
E (slightly stable)	4.21	0.12	294

Numerical results of Argon concentrations obtained by the CFD model have been compared with analytical expression of Pasquill theory and have been reported in Figures 4-10. In the following figures, the 2D distribution of the concentration is evaluated at different positions of the planes perpendicular to the wind direction (x) as depicted in Figure 3, and, in correspondence of the location (y,z) of the maximum value, 1D profile have been reported. The location of the chimney is considered at x=0, while the outlet of the chimney is located at (x=0 m, y= 500 m, z=102.2 m). In particular, Figures 4-6 show the normalized Argon concentration distributions at x=50 and at 200 m from the chimney as a function of y and z directions in correspondence of the maximum value of z and y, respectively.

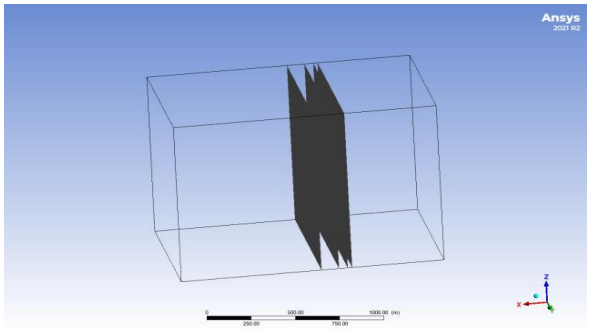

Figure 3. Plane sections yz at different x = 25, 50, 100, 200 m.

Results show a very good agreement only in the case of stability class D which is the neutral class, as depicted in Figure 5 and in Figure 7, where 2D spatial distributions of the normalized Argon concentration are represented. In other stability classes, as shown in Figures 4 and 6, the spatial distributions obtained by means of the CFD model present a less widespread behavior respect to the distribution obtained with the Pasquill theory, especially at higher distances from the chimney and these differences are more pronounced for the slightly unstable class C, as can be observed looking at Figure 8, where y distributions obtained at x=200 m have been reported for classes C, D, E both for CFD simulations and for the Pasquill theory. In all cases the spatial distribution obtained with CFD simulations are less widespread respect to the ones obtained with the Pasquill theory and the differences increase with the distance from the chimney, except for the stability class E in z direction.

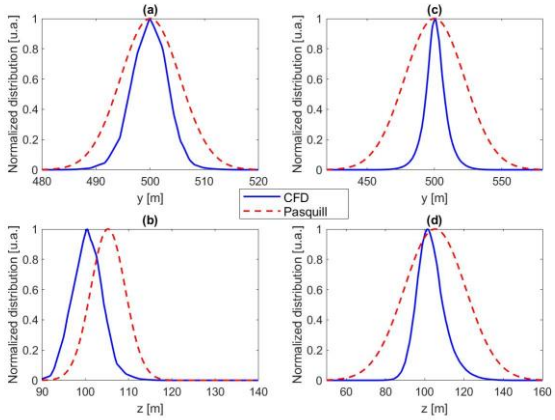

Figure 4. Argon concentration distribution in the case of stability class C on the yz plane section, at x = 50 m (a)-(b) and at x=200 m (c)-(d). Figures (a)-(c) along y direction and (b)-(d) along z direction.

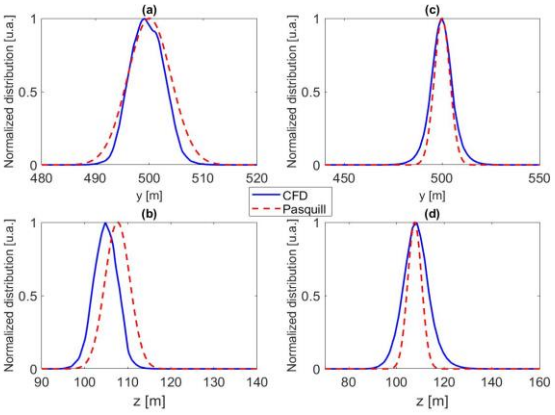

Figure 5. Argon concentration distribution in the case of stability class D on the yz plane section, at x = 50 m (a)-(b) and at x=200 m (c)-(d). Figures (a)-(c) along y direction and (b)-(d) along z direction.

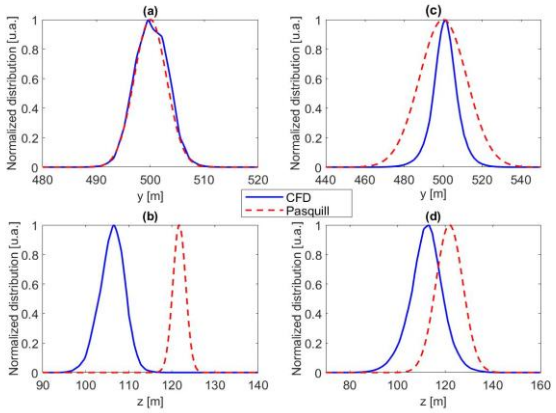

Figure 6. Argon concentration distribution in the case of stability class E on the *yz* plane section, at *x* = 50 m (a)-(b) and at *x*=200 m (c)-(d). Figures (a)-(c) along *y* direction and (b)-(d) along *z* direction.

More pronounced differences can be highlighted for the *z*-offset ΔH in the stability class E, while an acceptable agreement for the offset is obtained for the stability classes C and D.

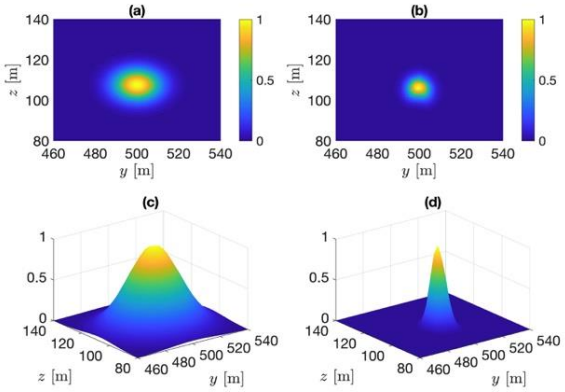

Figure 7. 2D Argon concentration distribution in the case of stability class D at *x* = 100 m Pasquill (a) and CFD (b) and at *x*=200 m Pasquill (c) and CFD (d).

The analytical offset in the framework of the Pasquill Theory depends from the stability class and it is calculated by using the following expressions [6, 16], in which expressions for different classes are reported:

$$\Delta H = 2.6\left(\frac{F}{S u_{wb}}\right)^{1/3} \quad \text{class E} \qquad (12)$$

$$\Delta H = 1.6\left(\frac{F^{1/3}\cdot X^{2/3}}{u_{wb}}\right) \quad \text{classes C, D} \qquad (13)$$

$$X = 49F^{0.625} \quad \text{classes C, D} \qquad (14)$$

$$S = 0.02\frac{g}{T_a}, \qquad F = gr^2 u_{Ar}\left(1-\frac{T_a}{T_s}\right) \qquad (15)$$

$$u_{wb} = \frac{u_s}{\kappa}\left[\ln\left(\frac{H}{z_0}\right)+5\left(\frac{H}{L}\right)\right] \quad \text{E} \qquad (16)$$

$$u_{wb} = \frac{u_s}{\kappa}\ln\left(\frac{H}{z_0}\right) \quad \text{D} \qquad (17)$$

$$u_{wb} = \frac{u_s}{\kappa}\left[\begin{array}{l}\ln\left(\frac{H}{z_0}\right)-2\ln\left(\frac{1+\chi}{2}\right)-\\ \ln\left(\frac{1+\chi^2}{2}\right)+\\ 2\arctan\chi-\frac{\pi}{2}\end{array}\right] \quad \text{C} \qquad (18)$$

$$\chi\left(\frac{H}{\bar{L}}\right) = \left(1-16\frac{H}{\bar{L}}\right)^{1/4} \qquad (19)$$

Where L=100 m, $\bar{L}$ = –230 m, u_s=0.12, 0.22, 0.42 m/s (respectively classes E, D, C), outlet velocity of Argon from the chimney u_{Ar}=5 m/s, chimney radius r=1 m, κ =0.41, z_o=0.03 m, H=102.2 m, T_a=297.13 K and T_s=300 K.

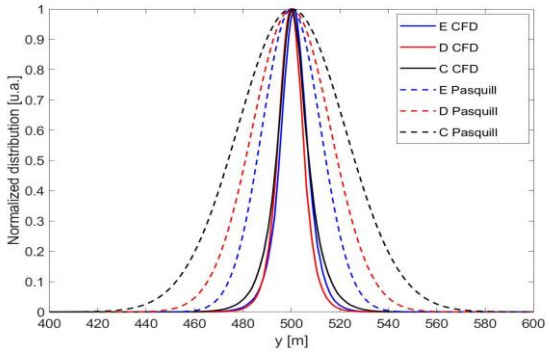

Figure 8. Argon concentration distribution for stability classes C, D and E, at *x* = 200 m, in correspondence of the location of the maximum value of the distribution in *z*.

In Figure 9, the full width at half maximum (FWHM), which represents the width of the distribution at its half maximum, is reported both in *y* and *z* direction as a function of the distance from the chimney. In all cases the spatial distribution obtained with CFD simulations are less widespread respect to the ones obtained with the Pasquill theory and the differences increase with the distance from the chimney, except for the stability class E in *z* direction, in whih an excellent agreement is observed.

The behavior of the offset in *z* direction can be observed in Figure 10, where Argon concentration distributions for stability classes C, D and E have been reported as a function of *z* at *x*=200 m, in correspondence of the maximum value of the distribution in *y* direction. Offset increases with the stability (from class C to E) and the same behavior occurs both in CFD and Pasquill profiles with a more pronounced difference for the stable class E.

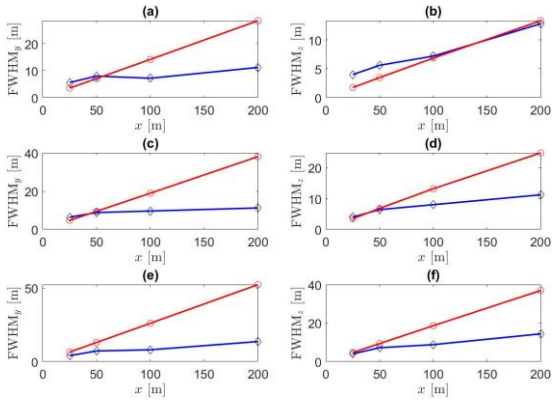

Figure 9. FWHM (Pasquill = red line and circle, CFD = blue line and diamond): (a) FWHM$_y$, Class E; (b) FWHM$_z$, Class E; (c) FWHM$_y$, Class D; (d) FWHM$_z$, Class D; (e) FWHM$_y$, Class C; (f) FWHM$_z$, Class C.

Offset increases with the stability (from class C to E) and the same behavior occurs both in CFD and Pasquill profiles with a more pronounced difference for the stable class E.

5. Conclusions

Nuclear medicine facilities and hadrontherapy centers [17] are situated in populated areas and GPM models can excessively overestimate submersion doses. For this reason, the correct estimation of a radioactive plume dispersion can be obtained with CFD models.

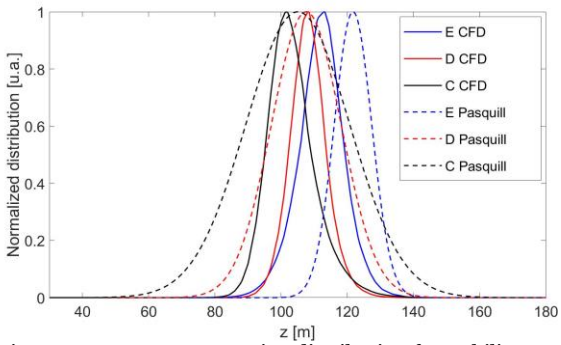

Figure 10. Argon concentration distribution for stability classes C, D and E, at x = 200 m, in correspondence of the location of the maximum value of the distribution in y.

In this paper a 3D CFD investigation of the dispersion of radioactive cloud emitted by a chimney in an open field has been carried out and numerical results have been compared with dispersion distributions given by the classical Pasquill expression. The fluid dynamic model has been solved in stationary condition, by considering Navier-Stokes (RANS) equation with k-ω SST model and a pressure-based mode calculation under a species transport scheme for incompressible fluids. Similarity theory (MOST) wind profiles have been included in boundary conditions. Numerical results are in good agreement with Pasquill especially in the case of stable classes so the presented CFD model can be considered as a viable option for pollutant transport. As future developments CFD calculations could be performed in the surroundings of an urban center, including the presence of buildings and obstacles which could change the velocity and the spatial distribution fields. This can be particularly useful for evaluations at short distances in urban areas where the hypothesis on the GPM plume cannot be applied.

References

1. Y. Kong, J. Zhang, S. Zhang, Y. Jiang, B. Wang, "CFD Numerical Simulation of Wind Field and Pollutant Dispersion in Valley Cities", *Research of Environmental Sciences,* **31**(3), 450-456, 2018. https://doi.org/10.13198/j-issn.1001-6929.2017.03.91
2. P. Qin, A. Ricci, B. Blocken, "CFD Simulations of Pollutant Dispersion in a Street Canyon: Impact of Ideal Versus Realistic Point Source Emissions", In *Proceedings of the 5th International Conference on Building Energy and Environment* (COBEE 2022), *Environmental Science and Engineering*, Springer, Singapore, pp. 33–39, 2023. https://doi.org/10.1007/978-981-19-9822-5_5
3. F. Pasquill, "Atmospheric Diffusion", John Wiley and Sons, New York, 1974.
4. Alan H. Huber, "Evaluation of a method for estimating pollution concentrations downwind of influencing buildings", *Atmos. Environ.*, **18**(11), 2313-2338, 1967. https://doi.org/10.1016/0004-6981(84)90003-9
5. M. Carestia et al., "Use of the "Hotspot" code for safety and security analysis in Nuclear Power Plants: A Case Study", *Environ. Eng. Manage. J.*, **15**(4), 905-912, 2016. https://doi.org/10.30638/eemj.2016.098
6. G.A. Briggs, "Diffusion estimation for small emissions", Preliminary report, United States, 1973. https://doi.org/10.2172/5118833
7. P.J Richards, R.P Hoxey, "Appropriate boundary conditions for computational wind engineering models using the k-ϵ turbulence model", *J. Wind Eng. Ind. Aerodyn.*, **46–47**, 145-153, 1993. https://doi.org/10.1016/0167-6105(93)90124-7
8. A. Sofachev, M. Kelly, M.Y. Leclerc, "Consistent two-equation closure modeling for atmospheric research: buoyancy and vegetation implementations", *Bound-Lay Meteorol*, **145**(2), 307–327, 2012. https://doi.org/10.1007/s10546-012-9726-5
9. F.R. Menter, M. Kuntz, R. Langtry, "Ten years of industrial experience with the SST turbulence model", *Turbul Heat Mass Transf*, 2003. Retrieved from: https://cfd.spbstu.ru/agarbaruk/doc/2003_Menter,%20Kuntz,%20Langtry_Ten%20years%20of%20industrial%20experience%20with%20the%20SST%20turbulence%20model.pdf
10. H.J. Breedt, K.J. Craig, V.D. Jothiprakasam, "Monin-Obukhov similarity theory and its application to wind flow modelling over complex terrain", *J. Wind Eng. Ind. Aerodyn.*, **182**, 308-321, 2018. https://doi.org/10.1016/j.jweia.2018.09.026
11. A. Castorrini, S. Gentile, E. Geraldi, A. Bonfiglioli, "Investigations on offshore wind turbine inflow modeling using numerical weather prediction coupled with local-scale computational fluid dynamics", *Renewable Sustainable Energy Rev.*, **171**, 113008 2023. https://doi.org/10.1016/j.rser.2022.113008

12. A.S. Monin, A.M. Obukhov, “Basic laws of turbulent mixing in the surface layer of the atmosphere”, Originally published in *Tr. Akad. Nauk SSSR Geophiz. Inst.*, **24**(151), 163-187, 1954. Retrieved from: https://gibbs.science/efd/handouts/monin_obukhov_1954.pdf
13. A.J. Dyer, “A review of flux-profile relationships”, *Boundary-Layer Meteorol.*, 7, 363–372, 1974. https://doi.org/10.1007/BF00240838
14. D. Golder, “Relations among stability parameters in the surface layer”, *Boundary Layer Meteorology*, **3**, 47–58, 1972. https://doi.org/10.1007/BF00769106
15. Ansys® ANSYS FLUENT 12.0 User’s Guide, 7.3.2 Using Flow Boundary Conditions release 12.0, ©ANSYS.Inc. 2009-01-29.
16. G.A. Briggs, “Plume rise and buoyancy effects, Atmospheric Science and Power Production”, ed. Randerson D., DOE/TIC 27601, Springfield, Department of Commerce, USA, 1984.
17. F. Bonforte, M. Ferrarini, A. D'Angola, E. Giroletti, D. Introini, “Heavy-ions shielding data for hadrontherapy application with Monte Carlo methods”, *Radiat. Prot. Dosim.*, **199**(17), 2061–2075, 2023. https://doi.org/10.1093/rpd/ncad207